Inorganica Chimica Acta xxx (xxxx) xxxx

Contents lists available at ScienceDirect

Inorganica Chimica Acta

journal homepage: www.elsevier.com/locate/ica

Research paper

A new heteropentanuclear complex containing the $[Fe_2^{III}Zn_3^{II}(\mu\text{-}OH)_3]$ structural motif as a model for purple acid phosphatases

Filipy Gobbo Maranha[a], Graciela Aparecida dos Santos Silva[a], Adailton J. Bortoluzzi[a], Ebbe Nordlander[b], Rosely A. Peralta[a,*], Ademir Neves[a,*]

[a] Universidade Federal de Santa Catarina, Departamento de Química, Laboratório de Bioinorgânica e Cristalografia – LABINC, Campus Universitário, Trindade, Florianópolis, SC 88040-900, Brazil
[b] Inorganic Chemistry Research Group, Chemical Physics, Center for Chemistry and Chemical Engineering, Lund University, Box 124, SE-221 00 Lund, Sweden

ARTICLE INFO

Keywords:
Pentanuclear complex
Hydrolase
Diesterase

ABSTRACT

Herein, we describe the synthesis and X-ray structure of a new heteropentanuclear complex (**2**) containing a $[Fe_2^{III}Zn_3^{II}(\mu\text{-}OH)_3]$ structural unit and the unsymmetrical ligand H_2L^2-et. The molecular structure of **(2)** shows that it is formed by a basic dinuclear $[Fe^{III}(\mu\text{-}OH)Zn^{II}(L^2\text{-}et)]$ unit that is connected to a second dinuclear $[Fe^{III}(\mu\text{-}OH)Zn^{II}(L^2\text{-}et)]$ unit through a hydroxo bridge while a third Zn^{II} ion is coordinated by the pendant 1,2-ethanediamine groups of H_2L^2-et, resulting in the pentanuclear complex. Kinetic studies on the hydrolysis of the substrate 2,4-BDNPP (bis(2,4-dinitrophenyl)phosphate) reveal that (**2**) shows diesterase activity. While the kinetic activity is comparable to the corresponding dinuclear $Fe^{III}Zn^{II}$ complex containing the same ligand, the association with 2,4-BDNPP is significantly decreased.

1. Introduction

There is considerable research interest concerned with systems inspired by the active site of the metalloenzymes purple acid phosphatases (PAPs) [1–8]. PAPs participate in numerous biological functions, including the bone turnover [1,3,9], and iron transport [10].

PAPs belong to the family of dinuclear metallohydrolases (Fe^{III}-M^{II}, where M = Fe, Zn, or Mn) and catalyze the hydrolysis of a variety of phosphoester bonds under acidic conditions. They are the only dinuclear metallohydrolases where the requirement of a mixed-valence form as the hydrolytically active site for catalysis has been clearly established [1].

To date, the crystal structures of PAPs originating from red kidney bean (rkbPAP) [7,8], rats [5,6], pigs [3,11], humans [7], and sweet potato [12] have been reported. In plant PAPs, the metal ion composition is predominantly Fe^{III}-M^{II} (M = Zn or Mn) centers [4,13–15]. In the structure of rkbPAP, the Zn^{II} ion is coordinated by two nitrogen atoms from histidine side-chains and one oxygen atom from an asparagine, and the Fe^{III} ion is coordinated by an oxygen atom from a tyrosine residue, a nitrogen atom from a histidine, and an aspartate. The Fe^{III}-M^{II} ions are bridged by two oxygen atoms, one from the carboxylate group of an aspartate and the other from a modeled μ-hydroxo group. Two oxygen atoms from a μ-1,3 phosphate group complete the coordination spheres of the Zn^{II} and Fe^{III} ions [16,17]. The two subunits in the plant PAPs are linked via a disulfide bridge [1]. Furthermore, metallohydrolases with a catalytic centre that accommodates more than two metal ions, while uncommon, were recently identified (i.e. PhoX and Rv0805). The enzyme PhoX is an extra-cytoplasmic alkaline phosphatase which contains five metal ions in its active site, comprising two antiferromagnetically coupled Fe^{III} ions and three Ca^{II} ions [18–20]. The diesterase Rv0805 from *Mycobacterium tuberculosis* contains as many as four metal ions in the active site, one similar to that of the other dinuclear metallohydrolases, and a Ca^{II}-specific one, which can bind in a site distinct from but close to the location that accommodates the transition metal ions and acts as an activator of the enzymatic activity [19,20].

The synthesis of small transition metal coordination complexes models (biomimetics) of the active site of PAPs has been pursued as a benchmark for the study of this system. Such biomimetics can potentially serve as structural and/or functional models aimed at gaining a better understanding of the structure and the action mode of the active site. In this regard many symmetrical [21–25] and unsymmetrical [16,24,26–32] ligands containing a bridging phenoxide moiety and different N/O donor atoms have been reported in the literature. Although much of the reactivity studies of the PAPs system have been performed with mixed-valence hetero-dinuclear complexes, we decided

* Corresponding authors.
E-mail addresses: rosely.peralta@ufsc.br (R.A. Peralta), ademir.neves@ufsc.br (A. Neves).

https://doi.org/10.1016/j.ica.2019.119280
Received 2 August 2019; Received in revised form 10 October 2019; Accepted 12 November 2019
Available online 13 November 2019

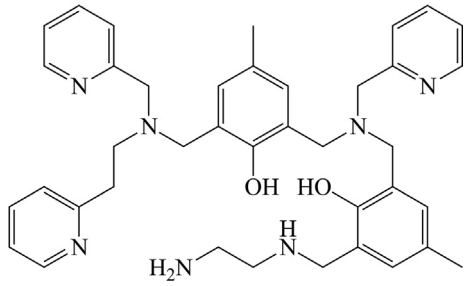

Chart 1. Structure of the ligand H_2L^2-et [27].

to explore the similar catalytic potential using a pentanuclear complex, with the objective of gaining insights on the metallohydrolases with catalytic centres that accommodate more than two metal ions [18–20]. Previous studies reported the synthesis of tetranuclear Fe^{III} [33,34] and Zn^{II} [23,33] complexes models of the PAPs.

Herein, we report a continuation of our research on the preparation of mixed-valence hetero-dinuclear Fe^{III}-M^{II} complexes as models for the active site of PAPs [16,24,25,27–29,35–41] and we describe the synthesis and X-ray structure of a new heteropentanuclear complex (**2**) containing the $[Fe_2^{III}Zn_3^{II}(\mu\text{-OH})_3]$ structural unit and the unsymmetrical ligand H_2L^2-et (Chart 1).

2. General procedures

All of the starting materials were purchased from Sigma-Aldrich, Acros, Merck, Riedel and Vetec.

2.1. Elemental analyses

Elemental microanalyses were performed with a C, H, N and S PerkinElmer analyzer (model 2400) using a PerkinElmer balance (model AD-4 Autobalance) and a tin capsule. Acetanilide (C_8H_9NO) was used as reference for calibrating the elemental analyzer, calcd: C, 71.09; H, 6.71; N, 10.36; O, 11.84. Found C, 71.16; H, 6.77; N, 10.39.

2.2. Infrared spectroscopy

Infrared spectra (Fig. S1) were obtained on a PerkinElmer Fourier transform infrared-attenuated total reflection (FTIR-ATR) spectrophotometer (model Spectrum 100) using a crystal of ZnSe (45°), and a TGS (triglycine sulfate) detector. The samples were analyzed directly with the crystal, averaging 18 scans in the range of 4000–400 cm^{-1} at a resolution of 4 cm^{-1}. The sample measurements were corrected with background measurements of the crystal alone without the samples. Room temperature was 25.0 ± 1.0 °C.

2.3. X-ray structure analyses

Crystallographic analysis of complex (**2**) was carried out with a single crystal Bruker KAPPA APEX II DUO diffractometer using graphite-monochromated MoKα radiation (λ = 0.71073 Å). Temperature of the sample was set at 150 (± 2) K with an Oxford Instruments Cryostream 700 series device. Crystals of complex (**2**) showed poor scattering power, so that the frames were collected with 30 s exposure by frame and with a maximum resolution of 0.83 Å. A total of 1420 frames were recorded with φ and ω scans method using the APEX2 software package [42]. All data were corrected for Lorentz and polarization effects and for absorption using the SADABS multi-scan method [42]. The structure was solved by direct methods and refined applying the full-matrix least-squares method using the SHELXS and SHELXL2014 programs [43], respectively. All non-hydrogen atoms were refined with anisotropic displacement parameters, except for a toluene solvate. Hydrogen atoms attached to carbon atoms were placed at their idealized positions with distances and U_{iso} taken from the default of the refinement program. The hydrogen atoms of the amine and hydroxo groups were found from a Fourier difference map and treated with a riding model. Hydrogen atoms of the disordered water solvate could not be located. Several atoms apart from the main metal complex entity (perchlorate counterions, acetonitrile and water solvate) have abnormal adp values; however, these atoms were refined anisotropically with positive definite tensors, but this generates several hard alerts in the checkcif report.

2.4. Mass spectrometry

The mass spectrum for (**2**) was obtained on a micrOTOF Q-II (Bruker Daltonics) equipped with an automatic syringe (K_D Scientific) for sample injection in the CEBIME (Centro de Biologia Molecular Estrutural) at the UFSC. The high-resolution positive ion ESI-MS analysis was carried out with acetonitrile/water (1:1 v/v) solution in a concentration of around 500 ppb. The mass spectrometer into which the samples were injected was operating with a constant flow rate of 3 μL min^{-1} and ultrapure solvent. The scan range was from *m/z* 150–1250. The simulated spectra were calculated using the Mmass software [44].

2.5. Ultraviolet–visible spectroscopy and spectrophotometric titration

The electronic absorption spectra and spectrophotometric titration were performed using a Perkin-Elmer Lambda 750 spectrophotometer in the range of 200–800 nm at 25 °C and quartz cuvettes with a capacity of 1 mL and optical path of 10 mm. The electronic absorption spectra were obtained with solutions of CH_3CN and CH_3CN/H_2O (1/1; v/v). The values of ε are given in L mol^{-1} cm^{-1}. The p*K*a values were determined by spectrophotometric titration, with experiment performed in 25 mL of a CH_3CN/H_2O (1/1; v/v) solution with ionic strength of 0.10 mol L^{-1} KCl in the pH range of 3.50–10.00 through the addition of aliquots of the 0.10 mol L^{-1} KOH solution. The pH was measured with a pH meter (model Oakton pH2700) and the p*K*w of the CH_3CN/H_2O (1/1; v/v) solution was 15.40 [45].

2.6. Square-wave voltammetry

The redox behavior of (**2**) was investigated by square-wave voltammetry using a Basi potentiostat/galvanostat (model Epsilon). The concentration of the complex was 1.0×10^{-4} mol L^{-1} in degassed CH_3CN solution (0.1 mol L^{-1}n-Bu_4NPF_6 as supporting electrolyte) at 25 °C, under an argon atmosphere. The electrolytic cell contained three electrodes: a glassy carbon working electrode; a platinum wire as a counter electrode and a Ag/AgCl reference electrode. Ferrocene was used as an internal standard. Scanning parameters: Step (4.0 mV), amplitude (25 mV) and frequency (15 Hz).

2.7. Reactivity measurements

The catalytic activity of (**2**) towards the activated phosphodiester bis(2,4-dinitrophenyl)phosphate (2,4-BDNPP) was evaluated spectrophotometrically on a Varian Cary50 Bio spectrophotometer, at 400 nm based on the appearance of the 2,4-dinitrophenylphenolate chromophore at 25 °C. The activated substrate 2,4-BDNPP was prepared as the pyridinium salt [46]. The effect of pH on the hydrolytic cleavage of 2,4-BDNPP was monitored in the pH range from 4.5 to 10.0. Reactions were performed using the following conditions: 750 μL freshly prepared aqueous buffer solution ($[buffer]_{final}$ 5.00×10^{-2} mol L^{-1}), buffer: 2-(*N*-morpholino)ethanesulfonic acid (MES; pH 4.00–6.50), 2-[4-(2-hydroxyethyl)-piperazin-1-yl]ethanesulfonic acid (HEPES; pH 7.00–8.50), *N*-cyclohexyl-2-aminoethanesulfonic acid (CHES; pH 9.00–10.00) with controlled ionic strength ($LiClO_4$) 0.10 mol L^{-1}; 100 μL of an acetonitrile complex solution ($[2]_{final}$ = 2.80×10^{-5} mol L^{-1}) and 550 μL of

acetonitrile were added to a 1 cm path-length cell. The reaction was initiated by the addition of 100 μL of an acetonitrile substrate solution ($[2,4\text{-BDNPP}]_{final} = 1.40 \times 10^{-3}$ mol L^{-1}) and monitored between 2% and 5% of reaction at 25 °C. The relevant molar absorption coefficients of the reaction product 2,4-dinitrophenolate (2,4-DNP) were determined at each pH under the same experimental conditions as those of the rate measurements [40]. The kinetic experiments under conditions of excess substrate were performed as follows: 750 μL of freshly prepared aqueous HEPES buffer solution (at pH 7.00), $[buffer]_{final} = 5.00 \times 10^{-2}$ mol L^{-1}, 100 μL of an acetonitrile complex solution ($[2]_{final} = 1.25 \times 10^{-5}$ mol L^{-1}) and 600–0 μL of acetonitrile were added to a 1 cm path-length cell. The reaction was initiated with the addition of 2,4-BDNPP solution ($[2,4\text{-BDNPP}]_{final} = 6.00 \times 10^{-4}$ to 7.80×10^{-3} mol L^{-1}). Correction for the spontaneous hydrolysis of 2,4-BDNPP was carried out by direct difference using a reference cell under identical conditions without adding the catalyst. The initial rate was obtained from the slope of the absorbance versus time plot over the first 10 min of the reaction. The conversion of the reaction rate units was carried out using ε = 12100 L mol^{-1} cm^{-1} for 2,4-DNP (at pH 7.00) and the initial concentration of the complex [40]. A kinetic treatment using the Michaelis–Menten equation approach was applied [47]. Isotopic effects of deuterium on the hydrolysis of 2,4-BDNPP promoted by complex (**2**) was evaluated following two reactions with identical conditions (vide experiments on the effect of pH) using the buffer solutions HEPES pH 7.00 (H_2O) and MES pD 6.60 (D_2O) to determine the relation k_H/k_D [9]. The reactions were monitored at 400 nm and 25 °C. The number of molecules of the substrate that are hydrolyzed per molecule of complex was monitored at 445 nm (ε = 3600 L mol^{-1} cm^{-1}) under a 50-fold substrate excess ($[2,4\text{-BDNPP}]_{final} = 2 \times 10^{-3}$ mol L^{-1}), relative to the complex ($[2]_{final} = 4 \times 10^{-5}$ mol L^{-1}), at pH 7.00 and 25 °C. The monoesterase-like activity of (**2**) was monitored with the monoester substrate, 2,4-dinitrophenyl phosphate (2,4-DNPP), directly with 1, 2, 4, 6, 8, 10 and 12 equivalents of 2,4-DNPP, and over a period of 5 h at 24 °C. After this time, 4 equivalents of the diester 2,4-BDNPP was added to the reaction mixture. Reactions were performed using freshly prepared aqueous buffer HEPES solution (at pH 7.00, $[buffer]_{final} = 5.00 \times 10^{-2}$ mol L^{-1}, $I_{final} = 5.0 \times 10^{-2}$ mol L^{-1} ($LiClO_4$), $[2]_{final} = 1.20 \times 10^{-4}$ mol L^{-1}). The monoester 2,4-DNPP was obtained as the lutidinium salt [49].

2.8. Synthesis

To a 30 mL methanolic solution of H_2L^2-et [27] (64.6 mg, 0.1 mmol, 645.84 g mol^{-1}) was added, under stirring, 74.5 mg (0.2 mmol, 372.38 g mol^{-1}) of $Zn(ClO_4)_2{\cdot}6H_2O$. To this solution was added, dropwise, a methanolic solution (30 mL) containing 0.1 mmol of Fe $(ClO_4)_3{\cdot}9H_2O$ (51.6 mg, 0.1 mmol, 516.33 g mol^{-1}) and 119.9 mg (3 mmol, 39.99 g mol^{-1}) of NaOH in 10 mL of water. The stirring was maintained for approximately 15 min and then $NaClO_4$ (122.4 mg, 1 mmol, 122.44 g mol^{-1}) was added. The solution was filtered off and left to stand. The resulting purple product was collected and washed with water, CH_2Cl_2 and diethyl ether (Yield: 45.3 mg, 20%). Single crystals suitable for X-ray analysis were obtained after recrystallization with 5 μmol of triphenylphosphine oxide and 5 μmol of (**2**) in 2 mL of the CH_3CN/CH_3OH/toluene (0.1/0.9/1; v/v) solution. Anal. Calc. for $C_{78}H_{93}N_{14}O_7Fe_2Zn_3(CH_3OH)_2(H_2O)_5(ClO_4)_5$: C, 41.81; H, 4.87; N, 8.53%. Found C, 41.64; H, 4.61; N, 8.17%. MM = 2297.91 g mol^{-1} FTIR-ATR, cm^{-1} (Fig. S1c): ν(OH) 3550; ν(C-H_{Ar} and C-H_{aliph}) 2959–2867; ν(C=N and C=C), 1610–1444; ν(C−O) 1276; ν(Cl-O) 1073; δ(C-H_{Ar}) 767; δ(C=C) 623.

3. Results and discussion

The reaction between the ligand H_2L^2-et [27] and stoichiometric amounts of $Zn(ClO_4)_2{\cdot}6H_2O$ and $Fe(ClO_4)_3{\cdot}6H_2O$ in the presence of six equivalents of NaOH and two equivalents of $NaClO_4$ in methanol leads to the stable heterodinuclear complex $[Fe^{III}(\mu\text{-OH})Zn^{II}(L^2\text{-et})](ClO_4)_2$ (**1**). This complex was characterized by spectroscopic methods (infrared and ultraviolet–visible), ESI-MS, elemental analysis and square-wave voltammetry [27]. Interestingly, when we increase the amounts of Zn $(ClO_4)_2{\cdot}6H_2O$, the unprecedented pentanuclear $[Fe_2^{III}Zn_3^{II}(\mu\text{-OH})_3(L^2\text{-et})_2](ClO_4)_5$ complex (**2**) with the unusual coordination of a third Zn^{II} ion by the pendant 1,2-ethanediamine groups of H_2L^2-et was obtained. After recrystallization with stoichiometric amounts of the triphenylphosphine oxide in CH_3CN/CH_3OH/toluene (0.1/0.9/1; v/v) solution, single crystals suitable for X-ray analysis were obtained. The triphenylphosphine oxide was used because it is a popular reagent to induce the crystallization of chemical compounds. Its rigidity and the basicity of the oxygen center make this species an alternative crystallization agent when it is difficult to crystallize molecules. This artifice is applicable to molecules that have acidic hydrogen atoms, e.g. phenols [50].

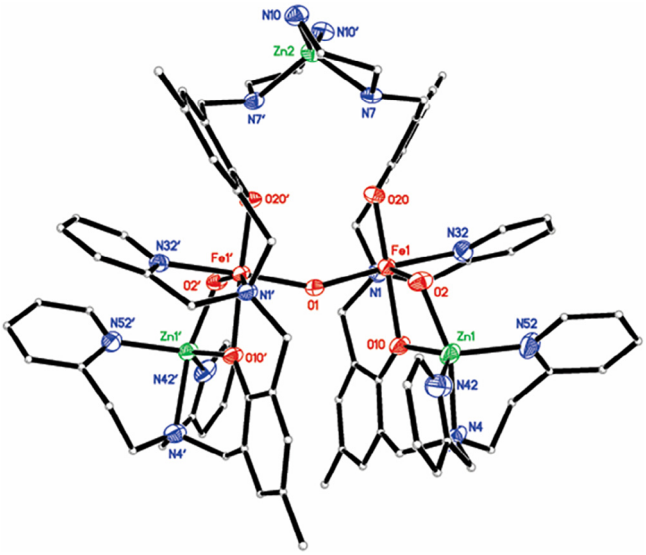

Fig. 1. ORTEP plot of the cation of complex (**2**). Hydrogen atoms were omitted for clarity.

Single purple crystals suitable for X-ray analysis were obtained after slow evaporation of complex (**2**) in an CH_3CN/H_2O (0.9/0.1; v/v) solvent mixture. The molecular structure of the pentanuclear cation in complex (**2**) is shown in Fig. 1.

It can be observed from the molecular structure of (**2**) that it is formed by two dinuclear $[Fe^{III}(\mu\text{-OH})Zn^{II}(L^2\text{-et})]$ units [27]. These units are connected through a hydroxo bridge while a third Zn^{II} ion is coordinated by the pendant 1,2-ethanediamine groups of H_2L^2-et, resulting in the pentanuclear complex. To the best of our knowledge, (**2**) represents a new example of a heteropentanuclear $[Fe_2^{III}Zn_3^{II}(\mu\text{-OH})_3(L^2\text{-et})_2]^{5+}$ cationic complex with this asymmetric structure. Crystallographic parameters for (**2**) are summarized in Table 1 and selected bond distances and angles are given in Table S1. In the structure of (**2**), the iron centers Fe(1) and Fe(1′) show an N_2O_4 coordination set and Zn(1) and Zn(1′) show an N_3O_2 coordination set. Both Zn ions possess distorted geometries intermediate between square pyramidal and trigonal bipyramidal with Addison parameters (τ) equal to 0.4945 and 0.58, for Zn(1) and Zn(1′), respectively [51]. The third zinc ion, Zn (2), shows an N_4 distorted tetrahedral coordination environment. In each half of the $[Fe_2^{III}Zn_3^{II}(\mu\text{-OH})_3(L^2\text{-et})_2]^{5+}$ cation, the Fe(1) and Fe (1′) ions are facially coordinated by the hard tridentate pendant arm of $(L^2\text{-et})^{-2}$ containing the amine (N1, N1′) and pyridine nitrogen (N32, N32′) and the phenolate oxygen (O20, O20′) atoms, while Zn(1) and Zn (1′) are coordinated by the soft side of $(L^2\text{-et})^{2-}$ through the amine (N4, N4′) and pyridine (N42, N52, N42′, N52′) nitrogen atoms. The bridging phenolate (O10, O10′) and the hydroxo (O2, O2′) oxygen atoms

Table 1
Crystal data and structure refinement for (**2**).

Empirical formula	$C_{87}H_{107}Cl_5Fe_2N_{15}O_{28.50}Zn_3$
Formula weight	2303.93
Temperature	150(2) K
Wavelength	0.71073 Å
Crystal system	Monoclinic
Space group	P $2_1/n$
Unit cell dimensions	a = 14.4012(15) Å b = 44.515(5) Å c = 16.5153(17) Å β = 111.2860(10)°
Volume	9865.2(18) Å^3
Z	4
Density (calculated)	1.551 Mg m^{-3}
Absorption coefficient	1.226 mm^{-1}
F(0 0 0)	4756
Crystal size	0.260 × 0.240 × 0.040 mm^3
Theta range for data collection	1.585 to 25.407°.
Index ranges	$-13 \le h \le 17$, $-53 \le k \le 52$, $-19 \le l \le 19$
Reflections collected	75,370
Independent reflections	18,147 (R_{int} = 0.0279)
Completeness to theta = 25.242°	100.0%
Absorption correction	Semi-empirical from equivalents
Max. and min. transmission	0.7452 and 0.6634
Refinement method	Full-matrix least-squares on F^2
Data/restraints/parameters	18,147/184/1282
Goodness-of-fit on F^2	1.121
Final R indices [I > 2sigma(I)]	R1 = 0.0617, w*R*2 = 0.1391
R indices (all data)	R1 = 0.0740, w*R*2 = 0.1450
Extinction coefficient	n/a
Largest diff. peak and hole	1.376 and −0.895 e Å^{-3}

complete the distorted bipyramidal N_3O_2 coordination of Zn(1) and Zn (1′) while the distorted octahedral N_2O_4 coordination of Fe(1) and Fe (1′) is complemented by the bridging phenolate oxygen (O10, O10′) and the bridging hydroxo groups (O2, O2′ and O1). The Zn(2) ion exhibits a distorted tetrahedral geometry with an N_4 donor set in which *N*-donors are provided by two secondary and two primary amine atoms of the 1,2-ethanediamine groups. The Fe-μ-OH (Fe(1)-O(2) = 1.935(3) Å; Fe(1)-O(1) = 1.971(3) Å; Fe(1′)-O(2′) = 1.937(3) Å; Fe(1′)-O (1) = 1.962(3) Å) and Zn-μ-OH (Zn(1)-O(2) = 1.984(3) Å; Zn(1′)-O (2′) = 2.008(3) Å; Zn(1′)-O(2′) = 1.937(3) Å; Zn(1′)-O(1) = 1.962(3) Å) distances in (**2**) are somewhat shorter than the corresponding metal-μ-OH distances in rkbPAP, which have been modeled to be between 2.0 and 2.2 Å. Furthermore, the $Fe^{+3}\cdots Zn^{+2}$ distances (Fe(1)-Zn (1) = 3.0967(9) Å and Fe(1′)-Zn(1′) = 3.0951(8) Å) are shorter but comparable to the distance of 3.20 Å found in rkbPAP [17].

The high-resolution positive ion ESI-MS for complex (**2**) (Fig. 2) was recorded in acetonitrile/water (1:1; v/v). A group of peaks at *m/z* 919.2 with a 2+ charge was observed. This signal can be assigned to the system $[Fe_2^{III}Zn_3^{II}(\mu\text{-}OH)_3(L^2\text{-}et)_2(CH_3O)_2(H_2O)_2(ClO_4)]^{2+}$, which corresponds to the molecular ion of complex (**2**) having three terminal

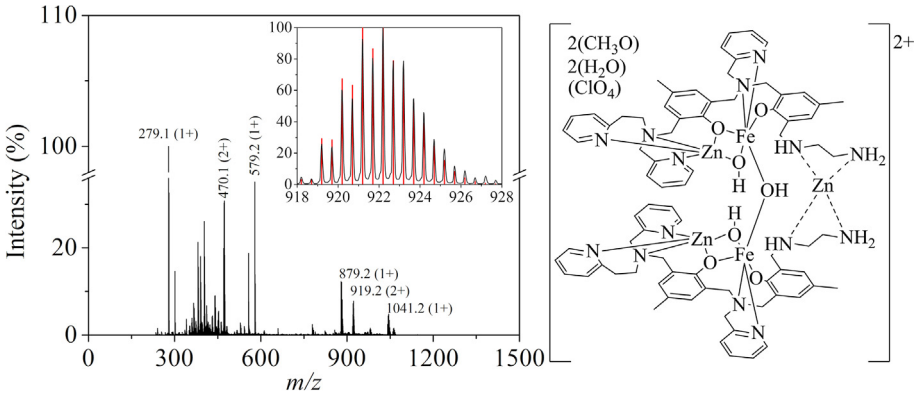

Fig. 2. The high-resolution positive ion ESI-MS spectrum of (**2**) in acetonitrile/water (1:1; v/v) solution and its isotopic distribution pattern. *m/z* = 919.1967 (experimental – black line) and *m/z* = 919.1975 (simulated – red line). Molecular formula: $[C_{78}H_{93}N_{14}O_7Fe_2Zn_3(H_2O)_2(CH_3O)_2\ (ClO_4)]^{2+}$. (For interpretation of the references to colour in this figure legend, the reader is referred to the web version of this article.)

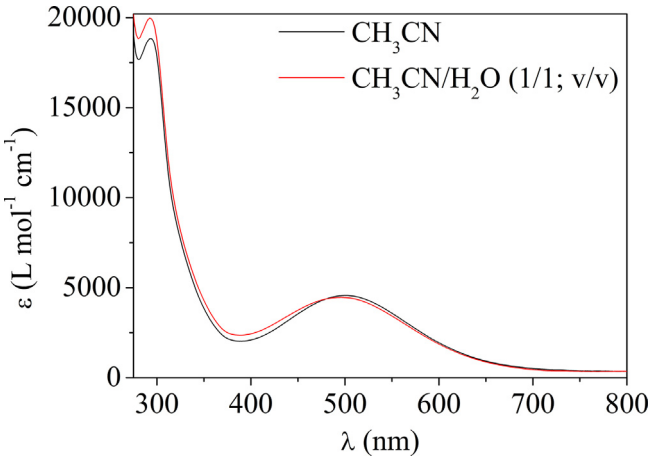

Fig. 3. Electronic absorption spectrum of complex (**2**) in CH_3CN and CH_3CN/H_2O (1/1; v/v). [2] = 1.5 × 10^{-3} mol L^{-1}. λ_{max} nm (ε mol^{-1} cm^{-1}) in the solvent: CH_3CN = 500 nm (ε = 4570 L mol^{-1} cm^{-1}) and 295 nm (ε = 18837 L mol^{-1} cm^{-1}); CH_3CN/H_2O (1/1; v/v) = 496 nm (ε = 4462 L mol^{-1} cm^{-1}) and 292 nm (ε = 19968 L mol^{-1} cm^{-1}).

hydroxo ions bound to the metal centers, two water molecules of hydration, two methoxide ions and one perchlorate counterion. In addition, peaks corresponding to fragmentation of the pentanuclear complex are also apparent, including peaks at *m/z* = 470.1, 879.2 and 1041.2 assigned to the dinuclear $[Fe^{III}(\mu\text{-}OH)Zn^{II}(L^2\text{-}et)(H_2O)_3(Li)(ClO_4)]^{2+}$, $[Fe^{III}(\mu\text{-}OH)Zn^{II}(L^2\text{-}et)(ClO_4)]^{+}$ and trinuclear $[Fe^{III}(\mu\text{-}OH)Zn^{II}(L^2\text{-}et)Zn^{II}(CH_3O)_2(H_2O)_2(ClO_4)]^{+}$ species, respectively. Peaks attributed to the fragments of the ligand ($[C_{15}H_{16}N_2O_2Na]^{+}$, *m/z* = 279.1; $[C_{32}H_{40}N_6O_3Na]^{+}$, *m/z* = 579.2) are also present.

The UV − vis absorption spectrum of complex (**2**) in CH_3CN/H_2O (1/1; v/v) solution shows an absorption band at 496 nm (ε = 4462 L mol^{-1} cm^{-1}, ca. 2200 L mol^{-1} cm^{-1} by dinuclear unit of the composition $[Fe^{III}(\mu\text{-}OH)Zn^{II}(L^2\text{-}et)]$), similar to the dinuclear complex (**1**) [27]), which is assigned to a ligand-to-metal charge transfer (LMCT) process, from the p_{π}(phenolate) → $d_{\pi^*}(Fe^{III})$. A second band was also observed at 292 nm (ε = 19968 L mol^{-1} cm^{-1}) which is attributed to the intra-ligand transition of the pyridine and phenolic rings (Fig. 3). The UV–Vis spectrum in acetonitrile is very similar, with an absorption band at 500 nm (ε = 4570 L mol^{-1} cm^{-1}) and a second one at 295 nm (ε = 18837 L mol^{-1} cm^{-1}), showing that in both media the species are the same.

The spectrophotometric titration (Fig. 4) in CH_3CN/H_2O (1/1; v/v) revealed two pK_a values for (**2**) (4.52 and 6.96). The first constant pK_{a1} can be attributed to the deprotonation of the Fe^{III}-bound H_2O water molecule (Scheme 1b), while pK_{a2} can be attributed to the deprotonation of the terminally coordinated water molecule at the Zn^{II} site (Scheme 1c) [52].

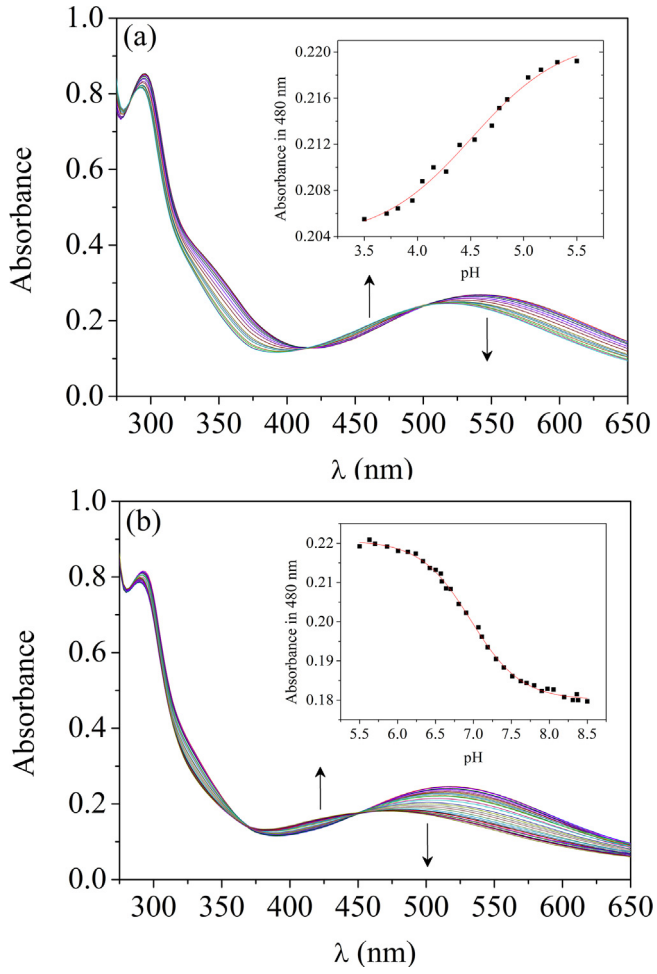

Fig. 4. Spectrophotometric titration in different pH ranges of ca. 3.5–5.5 (a) and 5.5–8.5 (b). Addition of 0.1 mol L^{-1} NaOH solution in a CH_3CN/H_2O (1/1; v/v) solution of complex (**2**) with I = 0.1 mol L^{-1} (KCl); [2] = 5.4×10^{-4} mol L^{-1}.

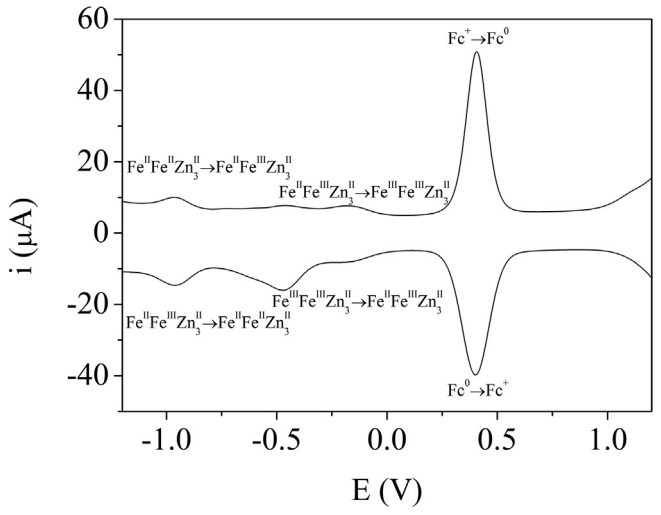

Fig. 5. Square-wave voltammogram of (**2**) ([2] = 1.0×10^{-4} mol L^{-1}) in CH_3CN solution and 0.1 mol L^{-1} n-Bu_4NPF_6 as supporting electrolyte. Electrodes: a glassy carbon working electrode; a platinum wire as a counter electrode and a Ag/AgCl reference electrode. Scanning parameters: Step (4.0 mV), amplitude (25 mV) and frequency (15 Hz).

These pK_a values are similar to those found for dinuclear Fe^{III}(μ-OH)Zn^{II} model complexes containing terminally bound Fe^{III}-OH_2 and Zn^{II}-OH_2 units [27,29].

The square-wave voltammogram (Fig. 5) of (**2**) in acetonitrile solution reveals two *quasi*-reversible redox processes: $E_{1/2}{}^1 = -0.468$ and $E_{1/2}{}^2 = -0.964$ V (relative to the ferrocenium/ferrocene couple) which are attributed to the $Fe^{III}Fe^{III}Zn_3{}^{II}/Fe^{II}Fe^{III}Zn_3{}^{II}$ and $Fe^{II}Fe^{III}Zn_3{}^{II}/Fe^{II}Fe^{II}Zn_3{}^{II}$ couples, respectively. The $E_{1/2}{}^2$ is in close agreement with the second redox (-0.89 V versus Fc^+/Fc) process observed for the dinuclear $Fe^{II}Fe^{III}$ complex containing the unsymmetrical ligand (BPBPMPF)$^{2-}$ [35].

Thus, we suggest that in pure CH_3CN solution the structural unit [Fe^{III}(μ-OH)Fe^{III}] is maintained as observed in the X-ray structure of (**2**). Nevertheless, it should be emphasized that the electrochemical behavior of (**2**) becomes much more difficult to interpret when square-wave voltammograms are obtained in CH_3CN/H_2O solution (not shown), most probably due to the equilibria proposed in Scheme 1.

We investigated the catalytic activity of complex (**2**) in the hydrolysis of the substrate 2,4-BDNPP (bis(2,4-dinitrophenyl)phosphate) by following spectrophotometrically the absorbance increase of the released 2,4-dinitrophenolate anion (λ_{max} = 400 nm), under conditions of excess substrate. The pH effect on the catalytic activity of complex (**2**) was evaluated from pH 4.5 to 10. The dependence of the initial rate on the pH shows a bell-shaped profile, with maximum activity around pH 7 (Fig. 6). This is similar to the results previously reported for other dinuclear Fe^{III}-Zn^{II} complexes with similar coordination environments [27,29] and to that found for rkbPAP [17].

The data were fitted using Eq. (S1) [34], with γ = 0.3, and a sigmoidal fit of the curve revealed pK_{a1} 4.88 and pK_{a2} 7.57, values which are in reasonable agreement with the results of pK_{a1} 4.52 and pK_{a2} 6.96 obtained from the spectrophotometric titration experiment. The pK_a values determined spectrophotometrically are lower than the kinetic pK_a values due to the absence of the substrate.

The shapes of the curves in Fig. 6 indicate that two active species are present in the pH range of 4.5–10: the first deprotonation step at pH ≅ 5 generates an active species; deprotonation of this species at pH ≅ 7.5

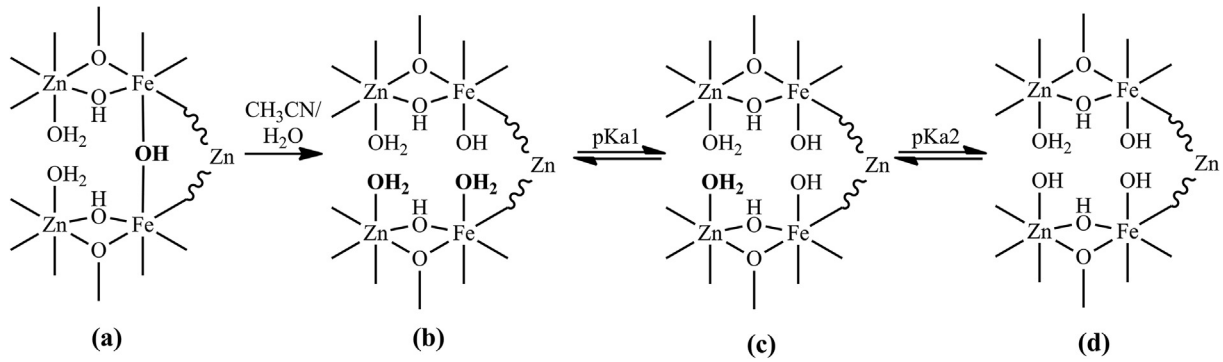

Scheme 1. Proposed equilibria for (**2**) in CH_3CN/H_2O (1/1; v/v) solution.

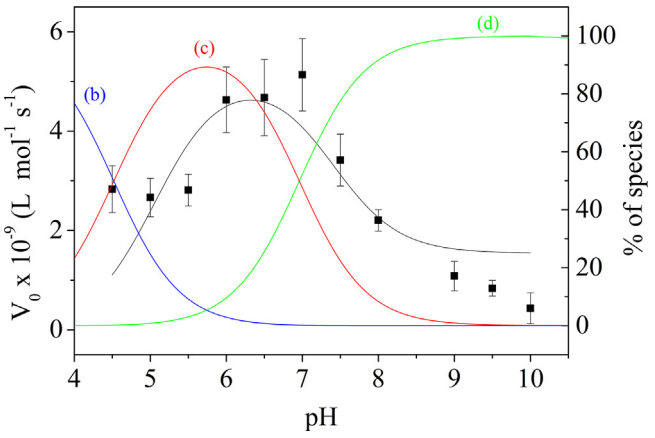

Fig. 6. Dependence of the initial reaction rate (V_0) on pH for the hydrolysis of 2,4-BDNPP enhanced by complex (**2**). Conditions: $[2]_{final} = 2.80 \times 10^{-5}$ mol L^{-1}; $[2,4\text{-BDNPP}]_{final} = 1.40 \times 10^{-3}$ mol L^{-1}; [buffer] = 5.0×10^{-2} mol L^{-1} (HEPES, pH = 7.00); $I = 5.0 \times 10^{-2}$ mol L^{-1} ($LiClO_4$) in CH_3CN/H_2O (1/1; v/v) at 25 °C. The distributions of the corresponding species (b), (c) and (d) (see Scheme 1) are shown as colored lines.

lowers its activity. The decrease in the activity upon deprotonation of Zn^{II}-H_2O indicates that the substrate replaces the bound H_2O. A hydroxide would be less labile than an aqua ligand, resulting in a lower leaving tendency of the Zn^{II}-OH group [31].

The dependence of the hydrolysis rate on the substrate concentration (2,4-BDNPP) was determined at pH 7.0, in which the most catalytically active species of complex (**2**) is present. The data presented in Fig. 7 shows saturation behavior and were analyzed using the Michaelis-Menten scheme. The Michaelis-Menten equation $v_0 = V_{max}([S]/([S] + K_M)$ was used to calculate the kinetic parameters k_{cat}, K_M and k_{cat}/K_M which are listed and compared with other PAP model complexes in Table 2.

The k_{cat} value for (**2**) is of similar magnitude when compared to heterodinuclear $Fe^{III}Zn^{II}$ complexes and lower than that of a tetranuclear Fe_4^{III} complex. In fact, the higher K_M value (lower association of the substrate) of (**2**) significantly decreases its catalytic efficiency (k_{cat}/K_M) under similar pH conditions [16,27]. At present we do not have a clear explanation for this behavior of (**2**) but steric constraints within the structure of the pentanuclear complex could contribute to

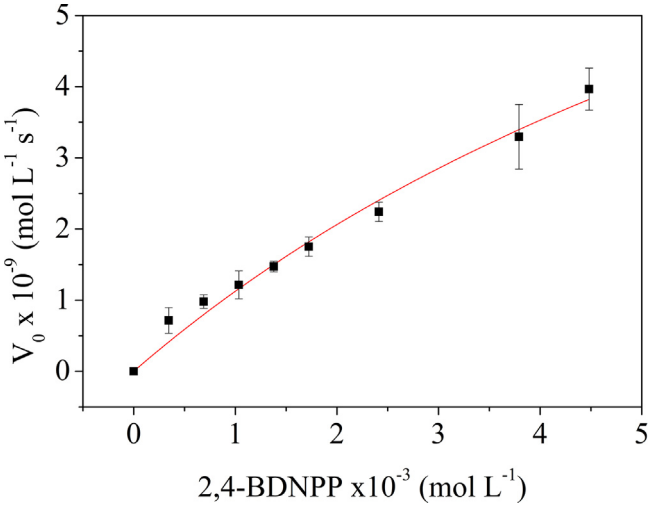

Fig. 7. Dependence of the initial reaction rate (V_0) on the 2,4-BDNPP concentration in the hydrolysis reaction promoted by complex (**2**). Conditions: $[2]_{final} = 1.25 \times 10^{-5}$ mol L^{-1}; $[2,4\text{-BDNPP}]_{final} = 6.00 \times 10^{-4}$ to 7.80×10^{-3} mol L^{-1}; $[buffer]_{final} = 5.0 \times 10^{-3}$ mol L^{-1} (HEPES, pH = 7.00); $I_{final} = 5.0 \times 10^{-2}$ mol L^{-1} ($LiClO_4$) in CH_3CN/H_2O (1/1; v/v) at 25 °C.

decreasing the association constant of the substrate. In the dinuclear species [27], the K_M value is of 1.61×10^{-3} mol L^{-1} while with the formation of the pentanuclear species and the presence of the third Zn^{II} ion the K_M value is of 9.85×10^{-3} mol L^{-1}. Although it was speculated that the presence of the third Zn^{II} may be a reflection of the catalytic activity in the case of complex (**2**), this metal may have a structural influence and catalytic relevance in the hydrolysis of the substrate 2,4-BDNPP (higher K_M and lower k_{cat}/K_M values). In this sense, the Rv0805 metallohydrolase is fully active in the "conventional" metal site, but the Ca^{II}-specific dinuclear site acts as a modulator of the activity of Rv0805. The Ca^{II} can bind in a site distinct from but close to the dinuclear transition-metal-ion binding site, and can alter the level of its reactivity depending on the presence or absence of Ca^{II} [19]. Finally, as shown in Table 2, complex (**2**) shows higher k_{cat} and k_{cat}/K_M values when compared with a tetranuclear Zn_4^{II} complex for which the same substrate (2,4-BDNPP) and pH optimum (8.5) were employed [23].

In order to elucidate the mode of interaction between 2,4-BDNPP and the pentanuclear complex (**2**), we followed the spectral change of the reaction mixture at pH 7.0 over a period of 24 h at 25 °C in the presence of excess substrate (Fig. S2). The intensity of the phenolate to Fe^{III} LMCT band (λ_{max} = 498 nm) is only slightly affected, thus strongly suggesting a monodentate coordination mode of the substrate to the Zn^{II} metal center. On the other hand, the absorption at ca. 400 nm continues to increase due to the formation of the product 2,4-dinitrophenolate (2,4-DNP).

We tested the activity of (**2**) in the hydrolysis of the monoester substrate 2,4-dinitrophenyl phosphate (2,4-DNPP) (Fig. S3); directly with 1, 2, 4, 6, 8, 10 and 12 equivalents of the 2,4-DNPP and over a period of 5 h at 24 °C only the background reaction was observed. After this time, 2,4-BDNPP was added to the reaction mixture and immediately the absorbance at 400 nm started to increase (Fig. S3), indicating that only the diester can be hydrolyzed. The number of catalytic cycles, estimated from a reaction that was monitored over 24 h at 25 °C and 445 nm (ε = 3600 L $mol^{-1}cm^{-1}$) with a 50:1 2,4-BDNPP/complex ratio, was found to be 9 turnovers. Furthermore, the measured kinetic isotope effect ($k_H/k_D \cong 0.8$) for (**2**) suggests that no proton transfer is involved in the rate-limiting step of the reaction [48].

Based on the X-ray structure, solution and kinetic studies, we propose a mechanism for the hydrolysis of 2,4-BDNPP by complex (**2**) as shown in Scheme 2. In the proposed mechanism at pH 7, the pentanuclear active species is composed of two dinuclear units of the composition [(HO)Fe^{III}(μ-OH)Zn^{II}(H_2O)(L^2-et)], connected to a third Zn^{II} ion by the 1,2-ethanediamine groups. The mechanism can be described analogously to the mechanism proposed in the literature [1,16,17,40,53] for dinuclear complexes, where the [(HO)Fe^{III}(μ-OH)Zn^{II}(H_2O)(L^2-et)] units of (**2**) are responsible for the hydrolysis of two 2,4-BDNPP substrate molecules. In brief, monodentate binding of the substrate to Zn^{II} is followed by a nucleophilic attack by the terminal, Fe^{III}-bound hydroxide and the concomitant release of 2,4-dinitrophenolate. The μ-1,3-coordinated DNPP intermediate undergoes substitution by water/OH^- molecules from the environment and regenerates the active site for the next catalytic cycle.

In summary, reaction of the dinucleating ligand (H_2L^2-et) with Zn$(ClO_4)_2{\cdot}6H_2O$ and Fe$(ClO_4)_3{\cdot}6H_2O$ results in the formation of the heterodinuclear [Fe^{III}(μ-OH)Zn^{II}(L^2-et)]$(ClO_4)_2$ complex (**1**), as expected [27]. However, in the presence of an excess of Zn$(ClO_4)_2{\cdot}6H_2O$, the recrystallization of this complex yields the unexpected pentanuclear [$Fe_2^{III}Zn_3^{II}$(L^2-et)$_2$(μ-OH)$_3$]$(ClO_4)_5$ complex (**2**), which has been structurally characterized. Complex (**2**) is a new heteropentanuclear $Fe_2^{III}Zn_3^{II}$ complex that is a functional model for the active site of PAPs, capable of cleaving diester bonds in the model substrate 2,4-BDNPP.

Declaration of Competing Interest

The authors declare that they have no known competing financial interests or personal relationships that could have appeared to

Table 2
Kinetic parameters of reported di- and tetranuclear iron and zinc model complexes for 2,4-BDNPP hydrolysis.

Complex	pH	k_{cat} (s^{-1})	K_M (mol L^{-1})	k_{cat}/K_M (mol^{-1} L s^{-1})	Ref
(**2**)	7.0	8.6×10^{-4}	$(9.85 \pm 3.49) \times 10^{-3}$	0.087	This study
(**1**)	7.0	$(11.2 \pm 5.56) \times 10^{-4}$	$(1.61 \pm 1.91) \times 10^{-3}$	0.696	[27]
$[L(OH_2)Fe^{III}$-$(\mu$-OH)$Zn^{II}]^{2+}$	6.5	9.13×10^{-4}	4.20×10^{-3}	0.217	[16]
$[Fe_4^{III}(HPBA)_2(\mu$-OAc$)_2(\mu$-O)-$(\mu$-OH$)(OH_2)_2]^{2+}$	6.5	$(16 \pm 0.2) \times 10^{-4}$	$(7.4 \pm 0.6) \times 10^{-3}$	0.216	[34]
$[Zn_4^{II}(TPPNOL)_2(OAc)_3]^{3+}$	8.5	1.28×10^{-4}	$(4.4 \pm 1) \times 10^{-3}$	0.029	[23]

(**1**) = H_2L^2-et = 2-(((2-aminoethyl)amino)methyl)-6-(((2-hydroxy-5-methyl-3-(((2-(pyridin-2-yl)ethyl)(pyridin-2-ylmethyl)amino)methyl)benzyl)(pyridin-2-ylmethyl)amino)methyl)-4-methylphenol.
(H_2L) = 2-bis[{(2-pyridylmethyl)-aminomethyl}-6-{(2-hydroxybenzyl)-(2-pyridyl methyl)}aminomethyl] −4-methylphenol.
H_3HPBA = 2-((2-hydroxy-5-methyl-3-((pyridin-2-ylmethylamino)methyl)benzyl)(2-hydroxybenzyl)amino) acetic acid.
HTPPNOL = *N,N,N*'-tris-(2-pyridylmethyl)-1,3-diaminopropan-2-ol.

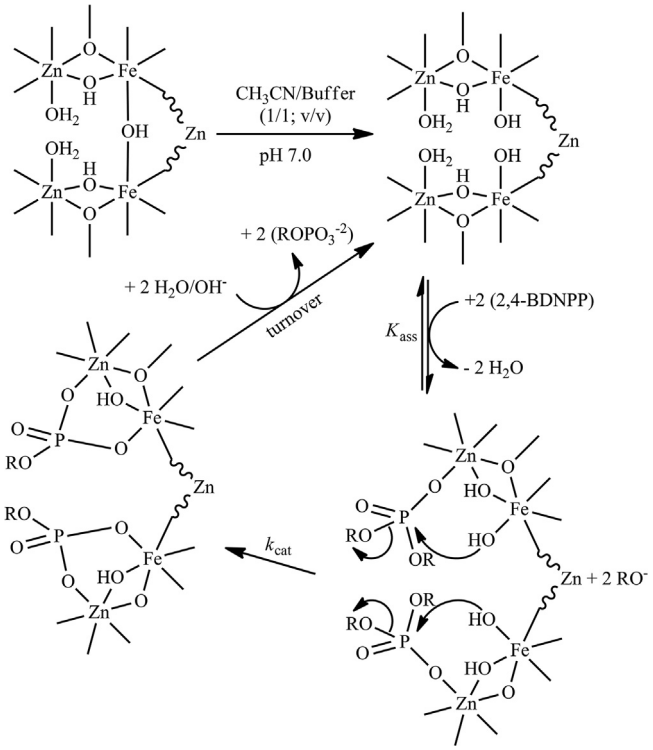

Scheme 2. Proposed mechanism for the hydrolysis of 2,4-BDNPP promoted by complex (**2**).

influence the work reported in this paper.

Appendix A. Supplementary data

Supplementary data to this article can be found online at https://doi.org/10.1016/j.ica.2019.119280.

References

[1] N. Mitić, S.J. Smith, A. Neves, L.W. Guddat, L.R. Gahan, G. Schenk, Chem. Rev. 106 (2006) 3338–3363, https://doi.org/10.1021/cr050318f.
[2] G. Schenk, N. Mitić, L.R. Gahan, D.L. Ollis, R.P. McGeary, L.W. Guddat, Acc. Chem. Res. 45 (2012) 1593–1603, https://doi.org/10.1021/ar300067g.
[3] C. Selleck, D. Clayton, L.R. Gahan, N. Mitić, R.P. McGeary, M.M. Pedroso, L.W. Guddat, G. Schenk, Chem. Eur. J. 23 (2017) 4778–4781, https://doi.org/10.1002/chem.201700866.
[4] G. Schenk, N. Mitić, G.R. Hanson, P. Comba, Coord. Chem. Rev. 257 (2013) 473–482, https://doi.org/10.1016/j.ccr.2012.03.020.
[5] J. Uppenberg, F. Lindqvist, C. Svensson, B. Ek-Rylander, G. Andersson, J. Mol. Biol. 290 (1999) 201–211, https://doi.org/10.1006/jmbi.1999.2896.
[6] Y. Lindqvist, E. Johansson, H. Kaija, P. Vihko, G. Schneider, J. Mol. Biol. 291 (1999) 135–147, https://doi.org/10.1006/jmbi.1999.2962.
[7] N. Sträter, B. Jasper, M. Scholte, B. Krebs, A.P. Duff, D.B. Langley, R. Han, B.A. Averill, H.C. Freeman, J.M. Guss, J. Mol. Biol. 351 (2005) 233–246, https://doi.org/10.1016/j.jmb.2005.04.014.
[8] D. Feder, L.R. Gahan, R.P. McGeary, L.W. Guddat, G. Schenk, ChemBioChem 20 (2019) 1536–1540, https://doi.org/10.1002/cbic.201900077.
[9] G.W. Oddie, G. Schenk, N.Z. Angel, N. Walsh, L.W. Guddat, J. de Jersey, A.I. Cassady, S.E. Hamilton, D.A. Hume, Bone 27 (2000) 575–584, https://doi.org/10.1016/S8756-3282(00)00368-9.
[10] P.R. Nuttleman, R.M. Roberts, J. Biol. Chem. 265 (1990) 12192–12199.
[11] L.W. Guddat, A.S. McAlpine, D. Hume, S. Hamilton, J. de Jersey, J.L. Martin, Structure 7 (1999) 757–767, https://doi.org/10.1016/S0969-2126(99)80100-2.
[12] G. Schenk, L.R. Gahan, L.E. Carrington, N. Mitić, M. Valizadeh, S.E. Hamilton, J. de Jersey, L.W. Guddat, Proc. Natl. Acad. Sci. 102 (2005) 273–278, https://doi.org/10.1073/pnas.0407239102.
[13] G. Schenk, Y. Ge, L.E. Carrington, C.J. Wynne, I.R. Searle, B.J. Carroll, S. Hamilton, J. de Jersey, Arch. Biochem. Biophys. 370 (1999) 183–189, https://doi.org/10.1006/abbi.1999.1407.
[14] A. Durmus, C. Eicken, B.H. Sift, A. Kratel, R. Kappl, J. Hüttermann, B. Krebs, Eur. J. Biochem. 260 (1999) 709–716, https://doi.org/10.1046/j.1432-1327.1999.00230.x.
[15] J.L. Beck, L.A. McConachie, A.C. Summors, W.N. Arnold, J. De Jersey, B. Zerner, Biochim. Biophys. Acta BBA – Protein Struct. Mol. Enzymol. 869 (1986) 61–68, https://doi.org/10.1016/0167-4838(86)90310-9.
[16] A. Neves, M. Lanznaster, A.J. Bortoluzzi, R.A. Peralta, A. Casellato, E.E. Castellano, P. Herrald, M.J. Riley, G. Schenk, J. Am. Chem. Soc. 129 (2007) 7486–7487, https://doi.org/10.1021/ja071184l.
[17] T. Klabunde, N. Sträter, R. Fröhlich, H. Witzel, B. Krebs, J. Mol. Biol. 259 (1996) 737–748, https://doi.org/10.1006/jmbi.1996.0354.
[18] S.C. Yong, P. Roversi, J. Lillington, F. Rodriguez, M. Krehenbrink, O.B. Zeldin, E.F. Garman, S.M. Lea, B.C. Berks, Science 345 (2014) 1170–1173, https://doi.org/10.1126/science.1254237.
[19] M.M. Pedroso, J.A. Larrabee, F. Ely, S.E. Gwee, N. Mitić, D.L. Ollis, L.R. Gahan, G. Schenk, Chem. Eur. J. 22 (2016) 999–1009, https://doi.org/10.1002/chem.201504001.
[20] M. Monteiro Pedroso, C. Selleck, J. Bilyj, J.R. Harmer, L.R. Gahan, N. Mitić, A.J. Standish, D.L. Tierney, J.A. Larrabee, G. Schenk, Dalton Trans. 46 (2017) 13194–13201, https://doi.org/10.1039/C7DT01350G.
[21] C. Pathak, D. Kumar, M.K. Gangwar, D. Mhatre, T. Roisnel, P. Ghosh, J. Inorg. Biochem. 185 (2018) 30–42, https://doi.org/10.1016/j.jinorgbio.2018.04.018.
[22] C. Pathak, M.K. Gangwar, P. Ghosh, Polyhedron 145 (2018) 88–100, https://doi.org/10.1016/j.poly.2018.01.029.
[23] L.L. Mendes, D. Englert, C. Fernandes, L.R. Gahan, G. Schenk, A. Horn, Dalton Trans. 45 (2016) 18510–18521, https://doi.org/10.1039/C6DT03200A.
[24] T.P. Camargo, F.F. Maia, C. Chaves, B. de Souza, A.J. Bortoluzzi, N. Castilho, T. Bortolotto, H. Terenzi, E.E. Castellano, W. Haase, Z. Tomkowicz, R.A. Peralta, A. Neves, J. Inorg. Biochem. 146 (2015) 77–88, https://doi.org/10.1016/j.jinorgbio.2015.02.017.
[25] A. Neves, M.A. de Brito, I. Vencato, V. Drago, K. Griesar, W. Haase, Inorg. Chem. 35 (1996) 2360–2368, https://doi.org/10.1021/ic950456v.
[26] C. Pathak, S.K. Gupta, M.K. Gangwar, A.P. Prakasham, P. Ghosh, ACS Omega 2 (2017) 4737–4750, https://doi.org/10.1021/acsomega.7b00671.
[27] G.A. dos S. Silva, A.L. Amorim, B. de Souza, P. Gabriel, H. Terenzi, E. Nordlander, A. Neves, R.A. Peralta, Dalton Trans. 46 (2017) 11380–11394, https://doi.org/10.1039/C7DT02035J.
[28] C. Pereira, G. Farias, F.G. Maranha, N. Castilho, G. Schenk, B. de Souza, H. Terenzi, A. Neves, R.A. Peralta, J. Biol, Inorg. Chem. 5 (2019) 675–691, https://doi.org/10.1007/s00775-019-01680-3.
[29] T.P. Camargo, A. Neves, R.A. Peralta, C. Chaves, E.C.P. Maia, E.H. Lizarazo-Jaimes, D.A. Gomes, T. Bortolotto, D.R. Norberto, H. Terenzi, D.L. Tierney, G. Schenk, Inorg. Chem. 57 (2018) 187–203, https://doi.org/10.1021/acs.inorgchem.7b02384.
[30] A.E. Roberts, G. Schenk, L.R. Gahan, Eur. J. Inorg. Chem. 2015 (2015) 3076–3086, https://doi.org/10.1002/ejic.201500351.
[31] S.J. Smith, R.A. Peralta, R. Jovito, A. Horn, A.J. Bortoluzzi, C.J. Noble, G.R. Hanson, R. Stranger, V. Jayaratne, G. Cavigliasso, L.R. Gahan, G. Schenk, O.R. Nascimento, A. Cavalett, T. Bortolotto, G. Razzera, H. Terenzi, A. Neves, M.J. Riley, Inorg. Chem. 51 (2012) 2065–2078, https://doi.org/10.1021/ic201711p.
[32] M. Jarenmark, M. Haukka, S. Demeshko, F. Tuczek, L. Zuppiroli, F. Meyer, E. Nordlander, Inorg. Chem. 50 (2011) 3866–3887, https://doi.org/10.1021/

ic1020324.
[33] N. Dutta, S. Haldar, G. Vijaykumar, S. Paul, A.P. Chattopadhyay, L. Carrella, M. Bera, Inorg. Chem. 57 (2018) 10802–10820, https://doi.org/10.1021/acs.inorgchem.8b01441.
[34] A. Kantacha, R. Buchholz, S.J. Smith, G. Schenk, L.R. Gahan, J. Biol. Inorg. Chem. 16 (2011) 25–32, https://doi.org/10.1007/s00775-010-0696-0.
[35] A. Neves, M. Aires de Brito, V. Drago, K. Griesar, W. Haase, Inorganica Chim. Acta. 237 (1995) 131–135, https://doi.org/10.1016/0020-1693(95)04678-3.
[36] A. Neves, L.M. Rossi, I. Vencato, W. Haase, R. Werner, J. Chem. Soc. Dalton Trans. 5 (2000) 707–712, https://doi.org/10.1039/A908062G.
[37] R. Jovito, A. Neves, A.J. Bortoluzzi, M. Lanznaster, V. Drago, W. Haase, Inorg. Chem. Commun. 8 (2005) 323–327, https://doi.org/10.1016/j.inoche.2005.01.007.
[38] B. de Souza, R. Heying, A.J. Bortoluzzi, J.B. Domingos, A. Neves, J. Mol. Catal. Chem. 397 (2015) 76–84, https://doi.org/10.1016/j.molcata.2014.11.006.
[39] A. Horn, I. Vencato, A.J. Bortoluzzi, R. Hörner, R.A.N. Silva, B. Spoganicz, V. Drago, H. Terenzi, M.C.B. de Oliveira, R. Werner, W. Haase, A. Neves, Inorganica Chim. Acta. 358 (2005) 339–351, https://doi.org/10.1016/j.ica.2004.09.021.
[40] R.A. Peralta, A.J. Bortoluzzi, B. de Souza, R. Jovito, F.R. Xavier, R.A.A. Couto, A. Casellato, F. Nome, A. Dick, R. Lawrence, G. Gahan, G.R. Schenk, F.C.S. de Hanson, E.C. Paula, S. de Pereira-Maia, P. Machado, P.C. Severino, C. Pich, T. Bortolotto, H. Terenzi, E.E. Castellano, A. Neves, M.J. Riley, Inorg. Chem. 49 (2010) 11421–11438, https://doi.org/10.1021/ic101433t.
[41] C. Piovezan, R. Jovito, A.J. Bortoluzzi, H. Terenzi, F.L. Fischer, P.C. Severino, C.T. Pich, G.G. Azzolini, R.A. Peralta, L.M. Rossi, A. Neves, Inorg. Chem. 49 (2010) 2580–2582, https://doi.org/10.1021/ic902489j.
[42] Bruker APEX2, SAINT and SADABS, version 2011.8-0; Bruker AXS Inc., Madison, Wisconsin, USA.
[43] G.M. Sheldrick, Acta Crystallogr. Sect. C Struct. Chem. 71 (2015) 3–8, https://doi.org/10.1107/S2053229614024218.
[44] M. Strohalm, D. Kavan, P. Novák, M. Volný, V. Havlíček, Anal. Chem. 82 (2010) 4648–4651, https://doi.org/10.1021/ac100818g.
[45] M.Á. Herrador, A.G. González, Talanta 56 (2002) 769–775, https://doi.org/10.1016/S0039-9140(01)00607-5.
[46] C.A. Bunton, S.J. Farber, J. Org. Chem. 34 (1969) 767–772, https://doi.org/10.1021/jo01256a001.
[47] D.L. Nelson, M.M. Cox, Principles of Biochemistry, Macmillan, New York, 2013.
[48] K.A. Deal, A.C. Hengge, J.N. Burstyn, J. Am. Chem. Soc. 118 (1996) 1713–1718, https://doi.org/10.1021/ja952306p.
[49] G. Rawji, R.M. Milburn, J. Org. Chem. 46 (1981) 1205–1206, https://doi.org/10.1021/jo00319a032.
[50] M.C. Etter, P.W. Baures, J. Am. Chem. Soc. 110 (1988) 639–640, https://doi.org/10.1021/ja00210a076.
[51] A.W. Addison, T.N. Rao, J. Reedijk, J. van Rijn, G.C. Verschoor, J. Chem. Soc., Dalton Trans. (1984) 1349–1356, https://doi.org/10.1039/DT9840001349.
[52] M. Lanznaster, A. Neves, A.J. Bortoluzzi, B. Szpoganicz, E. Schwingel, Inorg. Chem. 41 (2002) 5641–5643, https://doi.org/10.1021/ic025892d.
[53] A. Erxleben, Front. Chem. 7 (2019), https://doi.org/10.3389/fchem.2019.00082.